Brain and Behavior

Expression and immunolocalization of Gpnmb, a glioma-associated glycoprotein, in normal and inflamed central nervous systems of adult rats

Jian-Jun Huang, Wen-Jie Ma & Shigeru Yokoyama

Department of Biophysical Genetics, Kanazawa University Graduate School of Medicine, Kanazawa 920-8640, Japan

Abstract

Glycoprotein nonmetastatic melanoma B (Gpnmb) is a type I transmembrane protein implicated in cell differentiation, inflammation, tissue regeneration, and tumor progression. Gpnmb, which is highly expressed in glioblastoma cells, is a potential therapeutic target. However, little is known about its expression, cellular localization, and roles in non-tumorous neural tissues. In this study, we examined Gpnmb expression in the central nervous system of adult rats under both normal and inflammatory conditions. Reverse transcription-polymerase chain reaction analysis revealed that Gpnmb mRNA was expressed in the cerebrum, cerebellum, brain stem, and spinal cord of normal adult rats. Immunoperoxidase staining revealed that Gpnmb-immunoreactive cells were widely distributed in the parenchyma of all brain regions examined, with the cells being most prevalent in the hippocampal dentate gyrus, cerebellar cortex, spinal dorsal horn, choroid plexus, ependyma, periventricular regions, and in layers II and III of the cerebral cortex. Double immunofluorescence staining showed that these cells were co-stained most frequently with the microglia/macrophage marker OX42, and occasionally with the radial glia marker RC2 or the neuronal marker NeuN. Furthermore, an intraperitoneal injection of bacterial endotoxin lipopolysaccharide increased the number of Gpnmb and OX42 double-positive cells in the area postrema, which is one of the circumventricular organs, indicating infiltration of hematogenous macrophages. These results suggest that Gpnmb, which is expressed in microglia and macrophages in non-tumorous neural tissues, plays an important role in the regulation of immune/inflammatory responses.

Introduction

Glycoprotein nonmetastatic melanoma B (Gpnmb) is a type I transmembrane protein implicated in various biological processes, such as cell differentiation, inflammation, tissue regeneration, and invasion and metastasis of malignant tumors (Rose and Siegel 2010). Gpnmb contains a signal peptide and polycystic kidney disease I domain in its extracellular portion, a part of which is released in a soluble form during ectodomain shedding (Furochi et al. 2007a; Hoashi et al. 2010; Rose et al. 2010a). The cytoplasmic domain of Gpnmb contains potential interaction sites for a number of signaling molecules, including cyclin, mitogen-activated protein ki-

nase, and glycogen synthase kinase-3 (Selim 2009). Gpnmb is localized not only to the cell surface membrane, but also to endoplasmic reticulum microsomes in osteoblasts (Abdelmagid et al. 2008), melanosomes in melanoma cells (Hoashi et al. 2010), phagosomes in macrophages (Li et al. 2010), and cytoplasmic vesicles in renal tubule-derived MDCT cells (Patel–Chamberlin et al. 2011). Thus, Gpnmb is considered to function as a cell surface receptor, cell adhesion molecule, melanosomal protein, or soluble ligand (Selim 2009). To date, its orthologs such as dendritic cell heparan sulfate proteoglycan integrin-dependent ligand (DC-HIL; Shikano et al. 2001), osteoactivin (Safadi et al. 2002), or hematopoietic growth factor inducible

neurokinin-1 type (HGF-IN; Bandari et al. 2003) have been identified in different species. In order to avoid complexity, we hereafter use the term Gpnmb.

Since its initial identification in human melanoma cells (Weterman et al. 1995), Gpnmb has been considered a potential therapeutic target for malignant tumors. Its expression is upregulated in various tumor cells, including gliomas (Loging et al. 2000; Kuan et al. 2006; Tybruczy et al. 2010), hepatomas (Onaga et al. 2003), and breast cancer (Rose and Siegel 2010; Rose et al. 2010b). Gpnmb overexpression by virus-mediated gene transfer in a human glioma cell line resulted in a more invasive and metastatic phenotype, accompanied by enhanced expression of matrix metalloproteinase (MMP)-3 and MMP-9 (Rich et al. 2003). Tomihari et al. (2010) demonstrated using a mouse model that Gpnmb inhibits the activation of melanoma-reactive T lymphocytes and thereby promotes invasion. Moreover, an anti-Gpnmb monoclonal antibody that is conjugated with a cytotoxic agent has been subjected to clinical trials in patients with malignant glioma, breast cancer, and cutaneous melanoma (Tse et al. 2006; Pollack et al. 2007; Qian et al. 2008; Naumovski and Junutula 2010; Rose and Siegel 2010; Williams et al. 2010; Kuan et al. 2011).

In addition to tumor progression, Gpnmb is considered to function in non-tumorous tissues. Its expression is upregulated in damaged skeletal muscles (Furochi et al. 2007b), liver (Haralanova–Ilieva et al. 2005), and kidneys (Nakamura et al. 2007; Pahl et al. 2010; Li et al. 2010; Patel–Cahmberlin et al. 2011), and fractured bones (Abdelmagid et al. 2010). In vitro studies have shown that Gpnmb induces osteoblast and osteoclast differentiation (Selim et al. 2003; Selim et al. 2007; Abdelmagid et al. 2008; Sheng et al. 2008). In denervated mouse skeletal muscles, Gpnmb upregulates MMP-3 and MMP-9 in infiltrating fibroblasts (Ogawa et al. 2005). Gpnmb also functions as an inhibitor of T lymphocytes (Chung et al. 2007) and macrophages (Ripoll et al. 2007). These findings demonstrated the multiple roles of Gpnmb in normal tissues.

However, with regard to the nervous system, Gpnmb expression has been exclusively investigated in glioblastomas. Its expression in the normal brain is still unclear. Some studies steadily detected Gpnmb mRNA (Safadi et al. 2002; Onaga et al. 2003; Owen et al. 2003), but others not (Loging, et al. 2000; Shikano et al. 2001; Kuan et al. 2006). Moreover, little is known about the regional distribution and cellular localization of Gpnmb in the normal central nervous system (CNS). Therefore, we examined Gpnmb expression in CNS regions of normal adult rats by reverse transcription-polymerase chain reaction (RT-PCR) and immunohistochemical analyses. Furthermore, to gain insight into the role of Gpnmb in the non-tumorous CNS, we studied changes in Gpnmb expression in inflamed brains.

Materials and Methods

Experimental animals

Adult Wister rats (200–300 g) were purchased from Charles River Japan (Yokohama, Japan) and New Zealand white rabbits (approximately 4 kg) from CLEA Japan, Inc. (Tokyo, Japan). The experimental procedures approved by the Guideline for the Care and Use of Laboratory Animals in Kanazawa University. These animals were maintained in the Institute for Experimental Animals of Kanazawa University Advanced Science Research Center.

Injection of lipopolysaccharide (LPS)

LPS from *Escherichia coli* serotype O127:B8 (Sigma, St. Louis, MO) was dissolved in sterile phosphate-buffered saline (PBS; pH 7.4) and intraperitoneally injected at a dose of 0.1 mg/kg of body weight.

RT-PCR

cDNA encoding the entire protein-coding sequence of rat Gpnmb was obtained by RT-PCR using the following set of primers: 5′-AGAGTCAAGCCCTGACTGGC-3′ (forward 1) and 5′-GAAGAGTGGGTTCCCAGTCA-3′ (reverse 1). PCR was performed using a 50-μl reaction mixture containing cDNA prepared from injured sciatic nerve (Osamura et al. 2005; corresponding to 50 ng of total RNA), 1 × KOD FX buffer (Toyobo, Osaka, Japan), 200 μM dNTPs, 200 nM of each primer, and 1 unit of KOD FX DNA polymerase (Toyobo). The amplification consisted of 35 cycles of 10-sec denaturation at 98°C, 30-sec annealing at 60°C, and 2-min extension at 68°C. For TA cloning, 3′-A overhangs were added to the amplified product by treating it for 10 min at 72°C in a reaction mixture containing 1 × ExTaq buffer (Takara Shuzo, Otsu, Japan), 75 μM dNTPs, 2.5 mM MgCl$_2$, and 2.5 units of ExTaq DNA polymerase (Takara Shuzo). The resulting fragment was cloned into a pCR2.1-TOPO vector (Invitrogen, Carlsbad, CA) to yield pCRNMB, which was verified by nucleotide sequencing.

For analysis of regional mRNA distribution, rats were decapitated after deep anesthesia with diethyl ether and chloral hydrate (500 mg/kg, intraperitoneally), and various regions of CNS were dissected. Total cellular RNA was extracted by the acid-phenol guanidium thiocyanate-chloroform extraction method using RNA-Bee (Tel-Test, Friendswood, TX) and reverse-transcribed using a kit (First-Strand cDNA Synthesis Kit; Amersham Biosciences, Little Chalfont, Buckinghamshire, United Kingdom) in a 15-μl reaction mixture containing 1 μg of total RNA, 45 mM Tris (pH 8.3), 68 mM KCl, 15 mM dithiothreitol, 9 mM MgCl$_2$, 0.08 mg/mL bovine serum albumin (BSA), 10 μg/mL random hexanucleotide primers, and 1.8 mM dNTPs. After

incubation for 1 h at 37°C, the samples were diluted with distilled water (185 μl), and heated for 5 min at 100°C. PCR was performed in a 20-μl reaction mixture containing cDNA products (corresponding to 5 ng of total RNA), 1 × Ampdirect-G/C buffer (Shimadzu, Kyoto, Japan), 200 μM dNTPs, 200 nM of each primer, 2.5 mM $MgCl_2$, and 1 unit of Ex Taq DNA polymerase (Takara Shuzo). The primer pairs used were designed as follows (product size in parentheses): Gpnmb forward 2, 5′-TCCTCAGAGACCTCCCCATT-3′ and Gpnmb reverse 1 (993 bp); and glyceraldehyde 3-phosphate dehydrogenase (GAPDH) forward, 5′-TGAAGGTCGGTGTCAACGGATTTGGC-3′ and GAPDH reverse, 5′-CATGTAGGCCATGAGGTCCACCAC-3′ (983 bp). Amplification of Gpnmb and GAPDH cDNAs was performed for 35 and 30 cycles, respectively. Each cycle of the PCR program consisted of denaturation at 96°C for 30 sec, annealing at 60°C for 1 min, and extension at 72°C for 1 min. PCR products were electrophoretically separated on a 1.2% agarose gel and visualized by ethidium bromide staining.

Southern blot analysis

After electrophoresis, PCR products were transferred to a nylon membrane (Zeta-Probe; Bio-Rad Laboratories, Hercules, CA) and hybridized with horseradish peroxidase (HRP) conjugated probes. Probe labeling, hybridization, and detection were performed using the enhanced chemiluminescence (ECL) direct acid labeling and detection systems (GE Healthcare, Piscataway, NJ) according to the manufacturer's instructions. The probes used were the 460-bp *Nco*I (1194)/*Nco*I (1656) fragment from pCRNMB and the 490-bp *Nco*I (377)/*Apa*I (871) fragment from pCGAPDH (Osamura et al. 2005); numbers in parentheses are in accordance with the GenBank database (accession number NM_133298 for rat Gpnmb and X02231 for rat GAPDH) and represent the 5′-terminal nucleotide generated by restriction endonuclease digestion.

Antibody production and purification

A synthetic peptide corresponding to the C-terminal region of rat Gpnmb (amino acid residues 558–572, NCBI accession number NP_579832) was conjugated to keyhole limpet hemocyanin (1 mg peptide/mg carrier protein; Calbiochem, La Jolla, CA) using glutaraldehyde. Approximately 100 μg of peptide in complete Freund's adjuvant (Difco Laboratories, Detroit, MI) was subcutaneously inoculated into two New Zealand white rabbits. The rabbits were boosted every two weeks and bled five to seven days after each boost. For affinity-purification of the collected antisera, the peptide (1 mg) was coupled to Affi-Gel 10 (1 mL; Bio-Rad Laboratories) according to the manufacturer's protocol. Antiserum (5–10 mL) was incubated with the peptide-resin overnight at 4°C. After washing with 0.5 M $MgCl_2$, bound antibodies

were eluted with 4 M $MgCl_2$ and dialyzed against PBS (pH 7.4). Antibody concentration was determined by absorbance at 280 nm using 1.38 as the extinction coefficient.

Construction of an expression plasmid for rat Gpnmb

pCRNMB was digested with *Hin*dIII and *Eco*RV and treated with the Klenow fragment of DNA polymerase I. The resulting 1.9-kb fragment containing the entire protein-coding sequence of rat Gpnmb was ligated to *Xba*I-cleaved pEF-BOS (a generous gift from Professor Nagata, Kyoto University, Japan; Mizushima and Nagata 1990) after treatment with the Klenow fragment of DNA polymerase I to yield an expression plasmid, pEF-RNMB.

Transfection and immunofluorescence staining

COS-7 cells cultured in Dulbecco's modified Eagle's medium (Gibco-BRL, Grand Island, NY) containing 10% fetal calf serum in a 5% CO_2 atmosphere were transfected with pEF-RNMB or pEF-BOS by the DEAE-dextran method (Golub et al. 1989) and grown on poly-D-ornithine-coated glass coverslips. After two days, cells were washed with ice-cold PBS and sequentially incubated in (1) 2% paraformaldehyde (PFA) in 0.1 M phosphate buffer (PB; pH 7.4) for 30 min on ice; (2) PBS containing 0.3% Triton X-100 (PBS-T), three changes, 5 min each; (3) blocking solution (PBS-T containing 1% BSA and 1.5% normal goat serum) for 1 h at room temperature (RT); (4) affinity-purified anti-Gpnmb primary antibodies (0.3 μg/mL in the blocking solution) overnight at 4°C; (5) PBS-T, six changes, 5 min each; (6) fluorescein isothiocyanate (FITC) conjugated goat anti-rabbit IgG antibody (1:1000 in the blocking solution; Jackson ImmunoResearch Laboratories, West Grove, PA) for 1 h at RT; and (7) PBS-T, six changes, 5 min each. Next, coverslips were mounted on glass slides with Vectashield (Vector Laboratories, Burlingame, CA), sealed with nail polish and viewed under a epifluorescence microscope (IX71; Olympus, Tokyo, Japan) using U-MNIBA3 (excitation, 470–495 nm; emission, 515–550 nm) and U-MWU2 (excitation, 330–385 nm; emission, 420 nm) filter cubes for visualization of FITC and 4′,6-diamidino-2-phenylindole (DAPI), respectively. Digital images were acquired using a computer-linked camera (DP71; Olympus). The obtained images were processed using Adobe Photoshop CS2 (Adobe Systems, San Jose, CA).

Immunoblot analysis

Crude membranes were prepared from pEF-RNMB-transfected, pEF-BOS-transfected, or non-transfected COS-7 cells, and rat brains as follows. pEF-RNMB-transfected or pEF-BOS-transfected COS-7 cells (10 μg) and non-transfected cells were grown on 100-mm dishes as described

above. After two days, transfected and non-transfected cells were harvested by scraping in PBS containing 1% (w/v) EDTA, pelleted by centrifugation at $400 \times g$ for 10 min at 4°C, and stored at −80°C. The cell pellets and freshly dissected rat brains were homogenized in 3 mL of a solution containing 0.25 M sucrose, 1 mM EDTA (pH 8.0), and protease inhibitor cocktails (Complete Mini; Roche Applied Science, Mannheim, Germany) using a Teflon/glass homogenizer. The homogenates were centrifuged at $1600 \times g$ for 10 min at 4°C, and the supernatant was centrifuged at $84,000 \times g$ for 30 min at 4°C. The pellets were resuspended in 3 mL of 50 mM Tris-HCl and 1 mM EDTA and recentrifuged at $84,000 \times g$ for 30 min at 4°C. The obtained pellets were resuspended in 0.1% SDS. Protein concentration was estimated by the BCA protein assay kit (Thermo Scientific, Rockford, IL) using BSA as a standard. Membrane preparations (3 or 20 μg of protein) were fractionated on SDS-polyacrylamide gels and electrophoretically transferred to polyvinylidene difluoride membranes (Millipore, Bedford, MA). The membranes were stained with 0.1% Coomassie Brilliant Blue R-250 (CBB) containing 10% acetic acid and 40% methanol, photographed, and rinsed in 100% methanol. Next, the membranes were blocked for 1 h at RT in PBS containing 0.1% Tween 20, 5% skimmed dry milk, 1% BSA, and 5% normal horse serum, followed by overnight incubation at 4°C with anti-Gpnmb antibodies (0.3 μg/mL) in the blocking solution. The blots were

washed and incubated with HRP-conjugated donkey anti-rabbit IgG antibody (1:3000; GE Healthcare). Immunoreactive (IR) bands were detected by chemiluminescence on X-ray film (RX-U; Fuji Photo Film, Tokyo, Japan) using ECL reagents (GE Healthcare). Images were obtained using an image scanner (ES2200; Seiko Epson, Nagano, Japan) and Adobe Photoshop software.

Immunoperoxidase staining

Rats were transcardially perfused with PBS followed by perfusion with a fixative containing 4% PFA in 0.1 M PB after deep anesthesia with diethyl ether and chloral hydrate. Brains were removed immediately and postfixed in the same fixative overnight at 4°C and then cryoprotected for two days at 4°C with 30% sucrose in 0.1 M PB. Sections at a thickness of 16 or 18 μm were cut using a cryostat and collected in PBS. Free-floating sections were sequentially incubated in (1) blocking solution (PBS containing 0.3% Triton X-100, 1% BSA, and 1.5% normal goat serum) for 1 h at 4°C; (2) affinity-purified anti-rat Gpnmb antibodies (0.3 μg/mL in the blocking solution) overnight at 4°C; (3) PBS containing 0.3% Triton X-100, three changes, 5 min each; (4) biotinylated goat-anti rabbit IgG (1:2000; Vector Laboratories) in the blocking solution for 1 h at RT; (5) PBS containing 0.3% Triton X-100, three changes, 5 min each; (6) ExtrAvidin-Peroxidase (1:1000; Sigma) in PBS containing 0.3% Triton X-100 for

Table 1. List of antibodies used in this study.

Antibody	Species/Isotype	Source, Catalog number	Dilution	Immunogen
Primary antibody				
Calbindin D-28K	Mouse monoclonal IgG1	Swant, 300	1:100	Chicken gut-derived calbindin D28K
ED1 (CD68)	Mouse monoclonal IgG1	AbD Serotec, MCA341GA	1:100	Rat spleen cells
GFAP (Clone G-A-5)	Mouse monoclonal IgG1	Sigma, G 3893	1:400	Pig spinal cord-derived GFAP
NeuN	Mouse monoclonal IgG1	Millipore, MAB377	1:100	Purified cell nuclei from mouse brain
NG2	Mouse monoclonal IgG1	Millipore, MAB5384	1:100	Cell line expressing a truncated form of NG2
OX6 (MHC Class II Ia)	Mouse monoclonal IgG1	abcam, ab6403	1:400	Rat thymocyte membrane glycoprotein
OX42 (CD11b/c)	Mouse monoclonal IgG2a	abcam, ab1211	1:200	Rat macrophages
Radial glial cell marker-2 (Clone RC2)	Mouse monoclonal IgMλ	Millipore, MAB5740	1:200	Embryonic rat brain
S-100 (β-subunit; Clone SH-B1)	Mouse monoclonal IgG1	Sigma S 2532	1:1000	Bovine brain S-100β
Secondary antibody				
FITC-conjugated anti-rabbit IgG	Goat	Jackson ImmunoResearch, 111-095-144	1:500	
Texas Red-conjugated anti-mouse IgG	Goat	Molecular Probes, 00862	1:500	
Alexa Fluor 594-conjugated anti-mouse IgM	Goat	Molecular Probes, A21044	1:500	

30 min at RT; (7) PBS containing 0.3% Triton X-100, five changes, 5 min each; and (8) working solution of the metal-enhanced diaminobenzidine (DAB) substrate kit (Thermo Scientific). After six rinses in distilled water, sections were mounted on untreated clean glass slides and covered with mounting medium (Aquatex; Merck, Darmstadt, Germany) and a glass cover slip. Photomicrographs were obtained using a light microscope (BZ-8000; Keyence, Osaka, Japan). Negative controls were obtained by preadsorbing antibodies with an excess (30 mM) of the synthetic peptides.

Multiple-label immunofluorescence

Sections (16 μm) were prepared by the same method as for immunoperoxidase staining and sequentially incubated overnight at 4°C with rabbit anti-Gpnmb antibody (1 μg/mL) and mouse monoclonal antibodies in the blocking buffer; the details and final concentrations are given in Table 1. After rinsing, sections were incubated for 1 h at RT with a mixture of appropriate fluorescence-conjugated secondary antibodies (Table 1) in the blocking solution. Sections were examined under a Keyence BZ-9000 microscope using OP-66836 BZ filter GFP-BP (excitation, 440–470 nm; emission, 535–550 nm), OP-66838 BZ filter TexasRed (excitation, 540–560 nm; emission, 630–660 nm), and OP-66834 BZ filter DAPI-BP (excitation, 340–360 nm; emission, 450–460 nm).

Staining with isolectin B4 (IB4)

Sections were incubated with biotin-conjugated IB4 (1:100; Sigma) during primary antibody incubation and with Texas Red-conjugated streptavidin (1:100; GE Healthcare) during secondary antibody reaction.

Results

Gpnmb mRNA expression in rat brain

To examine whether Gpnmb mRNA was expressed in rat CNS, we first performed RT-PCR analysis. Primers were designed to distinguish between the amplified product from cDNA and an amplified product derived from contaminating genomic DNA. As shown in Fig. 1A, sense and antisense primers were made to recognize exons 6 and 11, respectively. PCR products from cDNA and genomic DNA were predicted to be 993 bp and 4.4 kb, respectively. Furthermore, specificity of PCR products was confirmed by Southern blot analysis using an internal probe (Fig. 1A). Gpnmb mRNA expression was detected in all brain regions examined; GAPDH cDNA was used to confirm the integrity of RNA preparations (Fig. 1B).

Antibody validation

To examine Gpnmb expression at the protein level, we generated a polyclonal antibody against rat Gpnmb by immuniz-
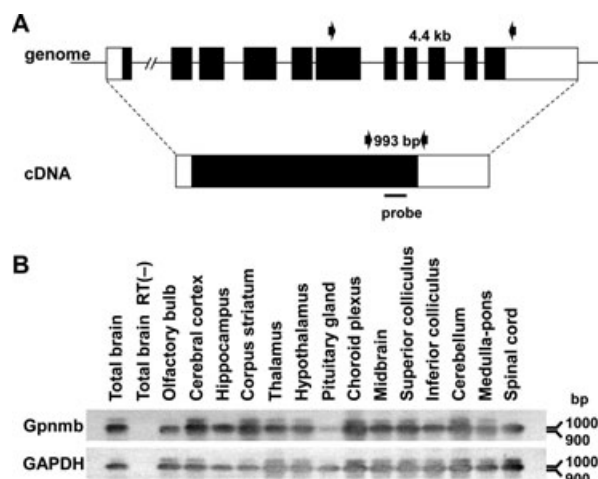
Figure 1. Reverse transcription-polymerase chain reaction (RT-PCR) analysis of Gpnmb mRNA in CNS of adult rats. (**A**) Schematic representation of the recognition sites of Gpnmb-specific PCR primers (arrows), the predicted sizes of the amplification products, and the probe used for Southern blot analysis. The exon–intron organization is depicted based on GenBank accession number NC_005103. Exons are indicated by rectangles and introns and 5′- and 3′-flanking regions are indicated by lines. Open and filled rectangles represent untranslated and protein-coding regions, respectively. (**B**) Photomicrographs of Southern blot analysis. Total cellular RNA from the indicated regions was subjected to RT-PCR. The amplified cDNAs were separated on 1.2% agarose gels, transferred to nylon membranes, and hybridized with HRP-conjugated Gpnmb- or GAPDH-specific probes. The absence of reverse transcriptase is indicated as [RT (-)]. GAPDH cDNA was amplified as a positive control. Size markers are given on the right.

ing rabbits with a synthetic peptide corresponding to the C-terminal region. Immunofluorescence staining revealed that Gpnmb-immunoreactivity (IR) was localized to lysosome-like structures in cDNA-transfected COS-7 cells, but not in mock-transfected or non-transfected cells (Fig. 2A). Immunoblot analyses using the obtained antibody detected a major band of 68 kD and a smear from 68 to 95 kD in cDNA-transfected COS-7 cells, but not in mock-transfected and non-transfected COS-7 cells (Fig. 2B). The 68 kD band agrees well with the predicted molecular mass of rat Gpnmb, and the smear is most likely a glycosylated form. Furthermore, the antibodies recognized two main bands of 68 and 150 kD in a crude membrane fraction prepared from the entire brain (Fig. 2C). These bands were completely abolished by preadsorption of the antibody with the peptide used for immunization (Fig. 2C).
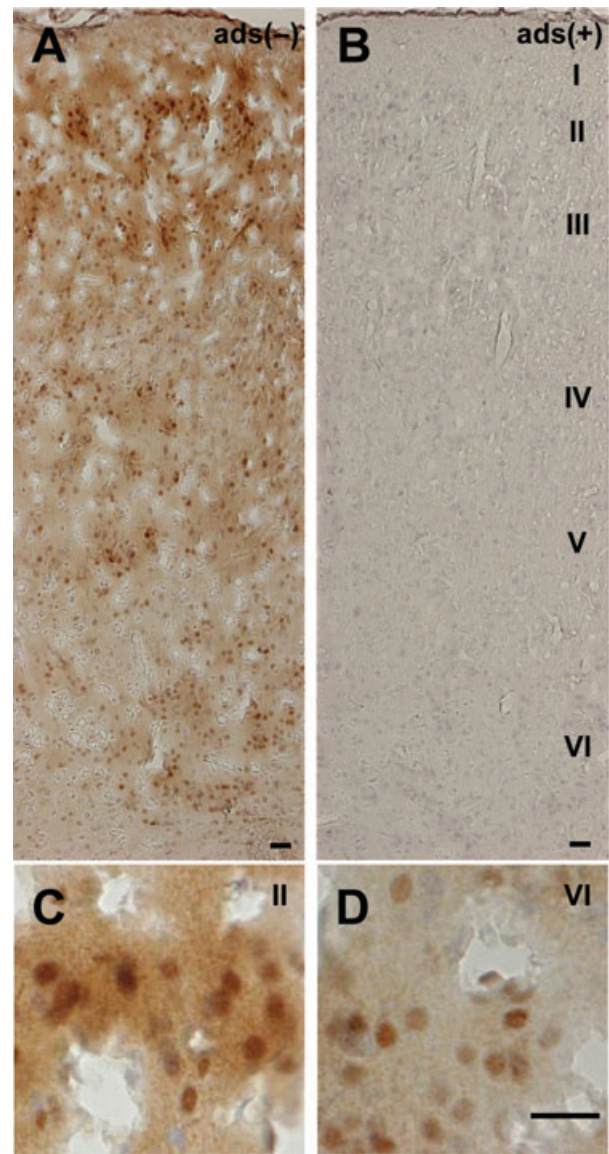
Gpnmb-IR in normal rat brain

Cerebral cortex

Gpnmb-IR was observed in all layers of the cerebral cortex, but staining was most prominent in layers II and III (Fig. 3A). IR was abolished by preadsorption of the primary
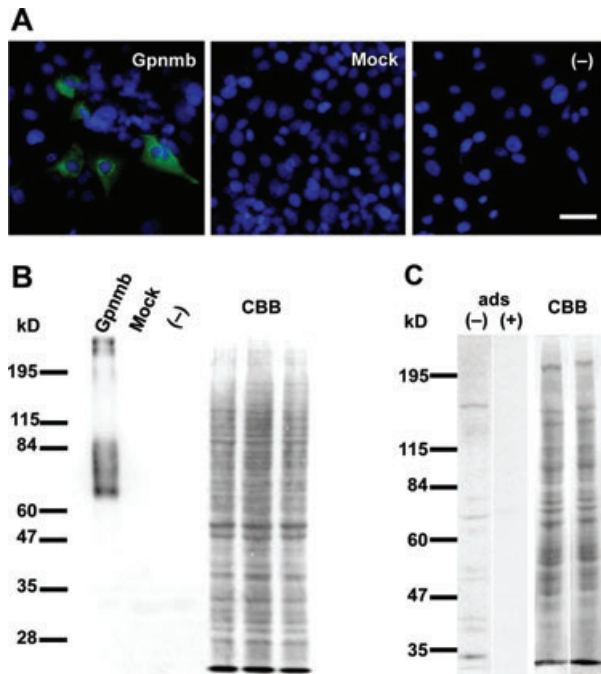
Figure 2. Antibody validation. (**A**) COS-7 cells that were transfected with an expression plasmid for Gpnmb (Gpnmb) or an empty vector (Mock) and non-transected cells (-) were stained with anti-Gpnmb antibody and visualized with FITC-conjugated secondary antibody (green). DAPI was used to stain cell nuclei (blue). Note that Gpnmb-immunoreactivity (IR) is detected only in Gpnmb cDNA-transfected cells. Scale bar, 50 μm. (**B**) Immunoblot showing reactivity of the antibody with rat Gpnmb expressed in COS-7 cells. The crude membranes (3 μg) obtained from Gpnmb cDNA-transfected, mock-transfected, and non-transfected COS-7 cells (-) were subjected to 9% SDS-PAGE, transferred to a nylon membrane, and probed with the anti-Gpnmb antibody prepared in this study. (**C**) Crude membranes from adult rat brains (20 μg) were subjected to 7.5% SDS-PAGE and transferred to a nylon membrane. The membrane was cut into two parts, and each was probed separately with the anti-Gpnmb antibody before and after adsorption (ads, – and ads, +) with the antigenic peptide. Membranes stained with CBB are presented as a loading control in both (**B**) and (**C**); the positions of molecular weight markers are indicated on the left.

Figure 3. Distribution of Gpnmb-IR in rat cerebral cortex. (**A, B**) Layers I–VI of the cortex. Sections obtained from adult rats were stained with anti-Gpnmb antibody before [**A,** ads (-)] or after [**B,** ads (+)] adsorption with the antigenic peptide and then visualized with DAB. (**C, D**) Higher magnification views of Gpnmb-IR cells in layers II and VI are shown, respectively. Scale bars: **A, B,** 50 μm; **C, D,** 30 μm.

antibody with the peptide used for immunization (Fig. 3B). Some of the Gpnmb-IR cells appeared to have fine processes (Fig. 3C, D). Double immunofluorescence staining revealed that Gpnmb-IR cells in layers II and III were positive for the microglia/macrophage markers OX42 (Fig. 4A) and IB4 (Fig. 4B). Although less frequently, some Gpnmb-IR cells were co-stained for the radial glial lineage marker RC2 (Fig. 4C). In contrast, no co-staining was observed with antibodies to the astrocyte lineage markers glial fibrillary acidic protein (GFAP; Fig. 4D) and protein S-100β (Fig. 4E) and the neuronal marker NeuN (Fig. 4F). This tendency was the same in other layers, except that occasional co-staining with NeuN was detected in layer VI (Fig. S1).

Hippocampus

Gpnmb-IR was observed throughout the hippocampus (Fig. 5A). IR was abolished by the primary antibody that was preadsorbed with the peptide used for immunization (Fig. 5B). IR in the CA1 segment (Fig. 5C) and dentate gyrus (Fig. 5F) was stronger than that observed in the CA2 and CA3 segments (Fig. 5D, E). With double fluorescence staining, Gpnmb-IR cells co-stained with OX42 or IB4 were observed
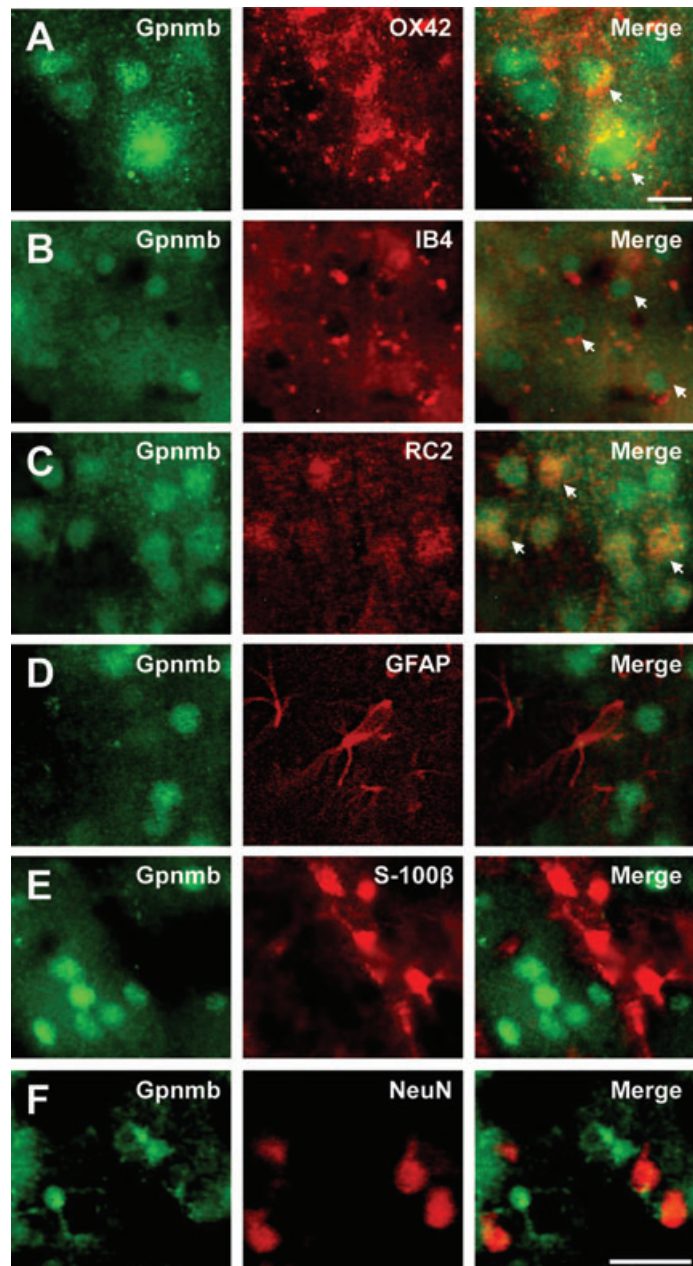
Figure 4. Characterization of Gpnmb-IR cells in cortical layers II–III with multiple markers. Sections were double-stained for Gpnmb (FITC, green) and the indicated markers (Texas Red, red). Note that Gpnmb-IR cells are co-stained with OX42, IB4, and RC2 (arrows). Scale bars: **A,** 10 μm; **B – F,** 30 μm.

in the polymorphic cell layer (Fig. 6A, B), but no co-staining with GFAP or NG2 was observed (Fig. 6C, D). A fraction of Gpnmb-IR cells in the granule cell layer of the dentate gyrus was positive for NeuN (Fig. 6E).

Cerebellum

In the cerebellum, cell bodies in the Purkinje cell layer and fine processes in the molecular layer were stained (Fig. 7A, C). Staining was abolished by preadsorbing the primary antibody with the peptide used for immunaization (Fig. 7B). The

Gpnmb-IR cells were co-stained with anti-GFAP (Fig. 7D) and anti-RC2 (Fig. 7E) antibodies, but not at all with an antibody against calbindin D-28K, a specific marker for Purkinje neurons (Fig. 7F). Therefore, we concluded that Gpnmb-IR cells were Bergmann glial cells.

Spinal cord

In the spinal cord, Gpnmb-IR was observed more frequently in the gray matter (Fig. 8A, C) than in the white matter (Fig. 8A, D). Staining was abolished when the primary
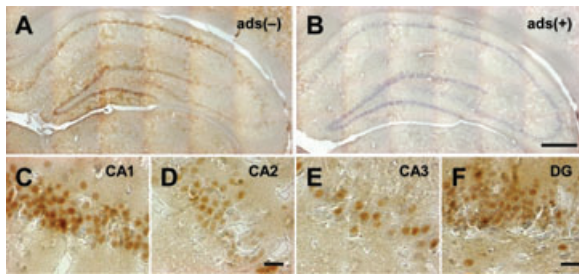
Figure 5. Distribution of Gpnmb-IR in rat hippocampus. (**A, B**) Low magnification images. Sections obtained from adult rats were stained with anti-Gpnmb antibody before [**A,** ads (-)] or after [**B,** ads (+)] adsorption with the antigenic peptide, and visualized with DAB. Continuous images were combined with Imagejoint program. (**C** – **F**) Immunoreactive cells in the indicated regions. Scale bars: **A, B,** 100 μm; **C** – **F,** 30 μm.

antibody was preadsorbed with the antigen peptide (Fig. 8B). In particular, intense staining was observed in the superficial layers of the dorsal horn and large neurons in the anterior and lateral horns (Fig. 8A, C). Gpnmb-IR cells in the dorsal horn were costained with OX42 (Fig. 8E) and NeuN (Fig. 8F).

Other areas

Prominent Gpnmb-IR was observed in the choroid plexus (Fig. 9A), ependyma (Fig. 9B), median preoptic nucleus (Fig. 9C), periventricular area surrounding the third ventricle (Fig. 9D), olfactory bulb (Fig. S2A–D), and striatum (Fig. S3A–C). These cells were confirmed to be positive for the microglia/macrophage markers in the choroid plexus (Fig. 9E), olfactory bulb (Fig. S2E, F), and striatum (Fig. S3C, D). The relative intensity of Gpnmb-IR in major regions of the rat CNS is summarized in Table S1.

Gpnmb-IR in inflamed rat brain

Since Gpnmb-IR cells in normal CNS were mostly positive for the microglia/macrophage lineage markers, we further examined whether inflammatory stimulation had any effects on these cells. After intraperitoneal injection of bacterial endotoxin (LPS), we observed that Gpnmb-IR in the area postrema was prominent compared with that in rats injected with PBS (Fig. 10A). This change became obvious 8 h after the LPS injection and was more widespread after 24 h (Fig. 10A). Gpnmb-IR cells were positive for OX42 (Fig. 10B) and appeared to be in contact with vessels (Fig. 10A, B). Gpnmb-IR was localized to cytoplasmic vesicles (Fig. 10B). These observations suggest that macrophages infiltrated from blood vessels in this systemic inflammation model.

Discussion

The main findings of this study were as follows: (1) Gpnmb mRNA was widely present in normal CNS of adult rats,
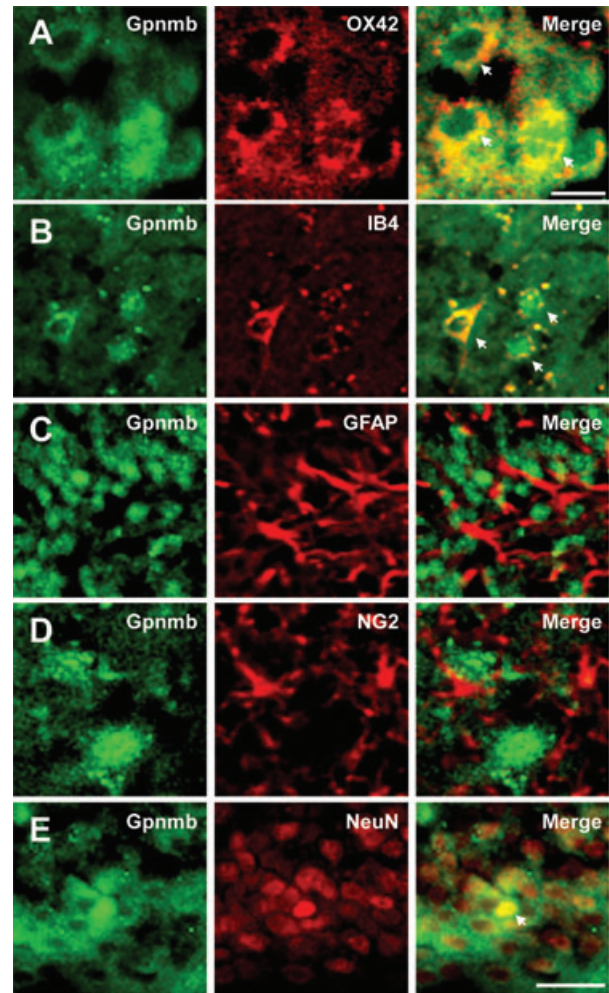

Figure 6. Characterization of Gpnmb-IR cells in the hippocampal dentate gyrus. Sections were double-stained for Gpnmb (green) and the indicated markers (red). Note that Gpnmb-IR cells were co-stained with OX42, IB4, or NeuN (arrows). Scale bars: **A,** 10 μm; **B** – **E,** 30 μm.

(2) Gpnmb-IR cells in the normal CNS are preferentially stained with microglia/macrophage markers, and occasionally with the radial glial marker RC2 and neuronal nuclei marker NeuN, and (3) systemic LPS administration evoked an increase in Gpnmb-IR in the area postrema. These data demonstrate for the first time that Gpnmb is expressed not only in brain tumor cells, but also in normal CNS and provide insights into the roles of Gpnmb in CNS.

Microglial cells are known to produce various cytokines, neurotrophic factors, proteases, and gaseous neuromodulators that regulate multiple processes, including maintenance of the CNS structure, immune/inflammatory responses, and regulation of neuronal networks (Kettenmann et al. 2011). Previous in vitro studies have demonstrated that Gpnmb can function as an anti-inflammatory regulator by inhibiting the activation of T lymphocytes (Chung et al. 2007) or by
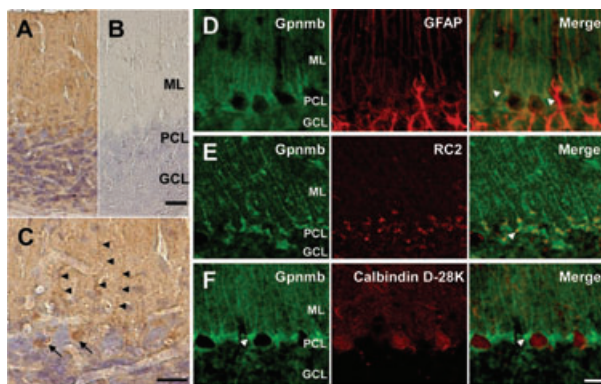
Figure 7. Gpnmb-IR in rat cerebellum. (**A – C**) Immunoperoxidase staining of rat cerebellar cortex. (**A, B**) Low magnification images. Sections obtained from adult rats were stained with the anti-Gpnmb antibody before [**A,** ads (-)] or after [**B,** ads (+)] adsorption with the antigenic peptide and then visualized with DAB. (**C**) Gpnmb-IR in cell bodies in the Purkinje cell layer and processes in the molecular layer are indicated by arrows and arrowheads, respectively. (**D – F**) Double immunofluorescence staining of rat cerebellar cortex. Sections from adult rats were double-stained for Gpnmb (green) and the indicated markers (red). Note that Gpnmb-IR is co-localized with GFAP (**D**) and RC2 (**E**) but not with calbindin D-28K (**F**). ML, molecular layer; PCL, Purkinje cell layer; GCL, granule cell layer. Scale bars: **A, B,** 30 μm; **C – F,** 20 μm.

reducing the secretion of proinflammatory cytokines from macrophages (Ripoll et al. 2007). Therefore, it is possible that Gpnmb produced by microglia acts on immune effector cells and alleviates excessive proinflammatory responses in the CNS.

In addition, we found that an intraperitoneal injection of LPS increased Gpnmb and OX42 double-positive cells in the area postrema. Because the increase was detectable 8 h after the injection, it is possible that blood-borne macrophages expressing Gpnmb infiltrated from systemic circulation and participated in the immune/inflammatory responses. The area postrema, which is an interface between the immune system and brain, contributes to autonomic control of brain-mediated host defense responses (Goehler et al. 2006). In previous studies, systemic LPS administration upregulated tumor necrosis factor-α (Breder et al. 1994) and interleukin-6 (Vallières and Rivest 1997) mRNA levels within 8 h. We assume that Gpnmb produced by infiltrating macrophages may counteract or decrease the actions of these proinflammatory cytokines.

Recently, a genome-wide association study identified the human Gpnmb gene on chromosome 7p15 as a risk locus for Parkinson's disease (International Parkinson's Disease Genomics Consortium (IPDGC) and Wellcome Trust Case Control Consortium 2 (WTTCCC2) 2011). Considering the present observation that Gpnmb-IR is detectable in ED1- or OX42-positive cells in the striatum (Fig. S3), it is tempting to
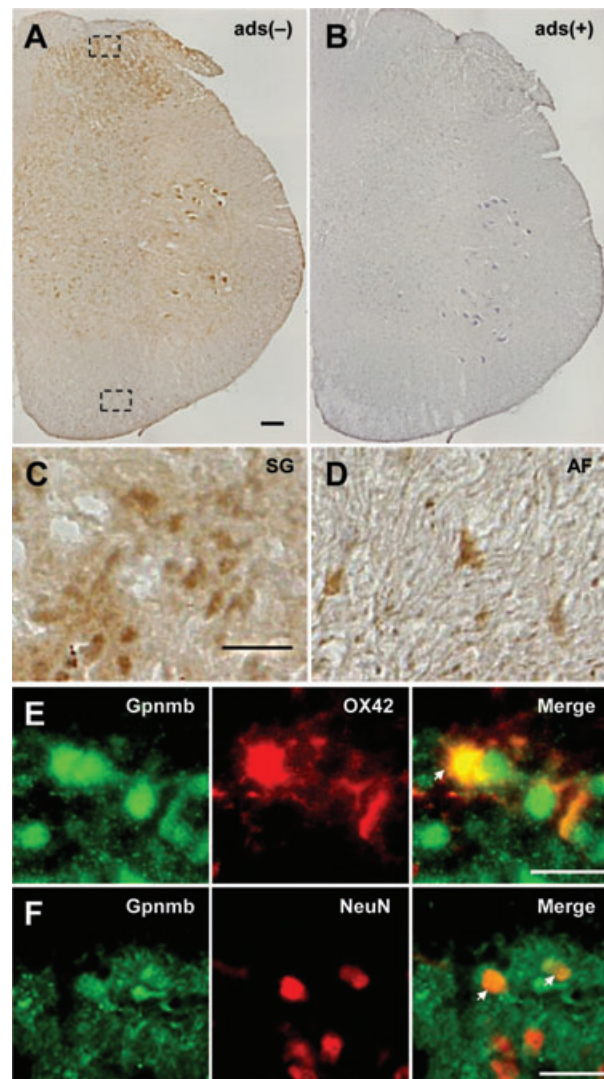
Figure 8. Distribution of Gpnmb-IR in rat spinal cord. (**A – D**) Immunoperoxidase staining before [**A,** ads (-)] or after [**B,** ads (+)] adsorption with the antigenic peptide. (**C, D**) Regions enclosed in the respective dotted line boxes (**A,** upper and lower) are high magnification views. SG, substantia gelatinosa; AF, anterior funiculus. (**E, F**) Double immunofluorescence staining. Gpnmb-IR cells are co-stained with OX42 (**E**) and NeuN (**F**), as indicated by arrows. Scale bars: **A, B,** 100 μm **; C – E,** 20 μm; **F,** 30 μm.

postulate that Gpnmb may exert an anti-inflammatory effect during the degeneration of nigrostriatal neurons.
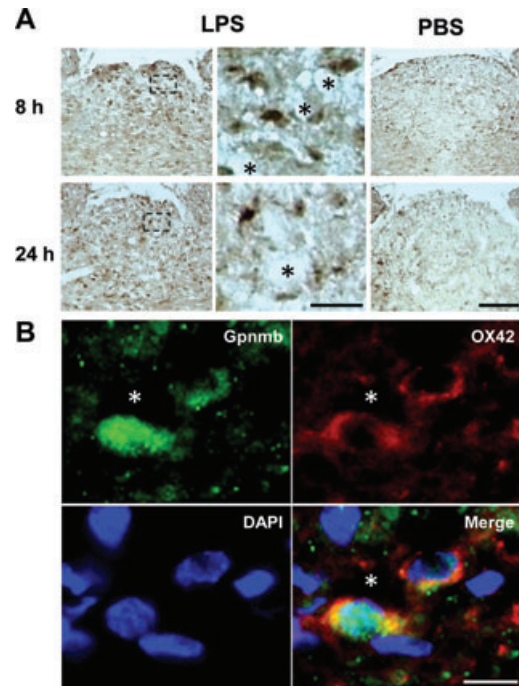
In addition to macrophage/microglia lineage cells, we detected Gpnmb-IR in ependymal, Bergmann glial, and NeuN-positive neuronal cells. Ependymal cells, like astrocytes, can be generated from radial glia (Spassky et al. 2005; Wang and Bordey 2008) and express GFAP (Doetsch et al. 1997; Liu et al. 2006; Wang and Bordey 2008). Bergmann glial cells are radial glia that persist in the adult cerebellum without
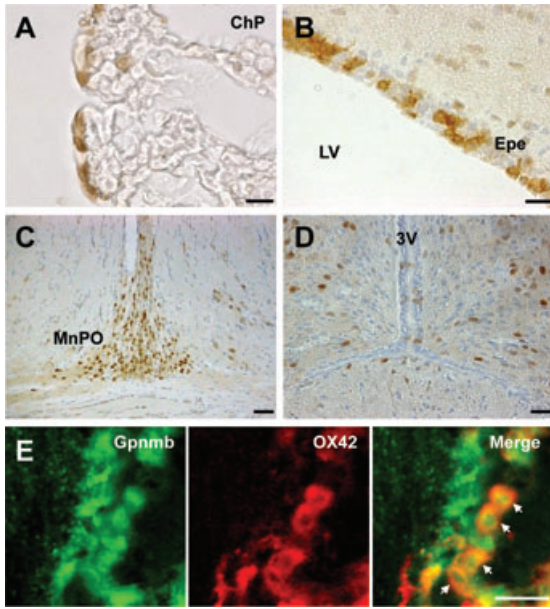
Figure 9. Gpnmb-IR in periventricular areas in rat brain. (**A**) Choroid plexus (ChP). (**B**) Ependymal cells (Epe). (**C**) Median preoptic nucleus (MnPO). (**D**) A region surrounding the third ventricle (3V). (**E**) Double immunofluorescence staining of the choroid plexus in the lateral ventricle. Gpnmb-IR cells are co-stained with OX42. Scale bars: **A, B, E,** 20 μm; **C,** 50 μm; **D,** 30 μm.

Figure 10. Gpnmb-IR in rat area postrema following endotoxin treatment. Adult rats were injected intraperitoneally with LPS or PBS. After 8 or 24 h, rats were perfused with fixative, and sections obtained were stained with anti-Gpnmb antibody. (**A**) Immunoperoxidase staining. Regions enclosed in dotted line boxes are high magnification views (LPS, right). Scale bars: LPS (left) and PBS, 50 μm; LPS (right) and PBS, 30 μm. (**B**) Triple immunofluorescence staining for Gpnmb (green), OX42 (red), and DAPI (blue). Asterisks denote vessels. Scale bar, 10 μm.

differentiating into mature astrocytes (Kriegstein and Götz 2003; Rakic 2003; Wang and Bordey 2008) and regarded as specialized astrocytes (Rakic 2003). Although these GFAP-positive cells are originated from radial glia, Gpnmb-IR was detected only in ependymal and Bergmann glial cells, but not in the majority of astrocytes. One possible explanation for this difference is that Gpnmb expression in ependymal and Bergmann glial cells may take place after commitment to terminal differentiation. Although the nature and ontogenic origin of Gpnmb and NeuN double-positive cells are currently unclear, Gpnmb-IR in hippocampal granular cell neurons could be explained as a remnant of radial glia, from which these neurons originated (Kriegstein and Götz 2003). Elucidation of the role of Gpnmb in these cell types requires more detailed characterization during development.

In conclusion, the present results indicate that Gpnmb was expressed in microglia/macrophage and radial glial lineage cells in non-tumorous neural tissues. It is therefore conceivable that Gpnmb-targeted therapies may have detrimental effects on these cell types. More importantly, our findings raise the possibility that Gpnmb may serve as a novel regulator of immune/inflammatory responses in CNS. Future studies are needed to clarify the role of Gpnmb in immune/inflammatory responses underlying traumatic nerve injury and neurodegenerative diseases, such as multiple sclerosis, Parkinson's disease, and Alzheimer's disease.

Acknowledgments

References

Abdelmagid, S. M., M. F. Barbe, M. C. Rico, S. Salihoglu, I. Arango-Hisijara, A. H. Selim, M. G. Anderson, T. A. Owen, S. N. Popoff, and F. F. Safadi. 2008. Osteoactivin, an anabolic factor that regulates osteoblast differentiation and function. Exp. Cell Res. 314:2334–2351.

Abdelmagid, S. M., M. F. Barbe, M. Hadjiargyrou, T. A. Owen, R. Razmpour, S. Rehman, S. N. Popoff, and F. F. Safadi. 2010. Temporal and spatial expression of osteoactivin during fracture repair. J. Cell. Biochem. 111:295–309.

Bandari, P. S., J. Qian, G. Yehia, D. D. Joshi, P. B. Maloof, J. Potian, H. S. Oh, P. Gascon, J. S. Harrison, and P. Rameshwar. 2003. Hematopoietic growth factor inducible neurokinin-1 type: a transmembrane protein that is similar to neurokinin 1 interacts with substance P. Regul. Pept. 111:169–178.

Breder, C. D., C. Hazuka, T. Ghayur, C. Klug, M. Huginin, K. Yasuda, M. Teng, and C. B. Saper. 1994. Regional induction of tumor necrosis factor α expression in the mouse after systemic lipopolysaccharide administration. Proc. Natl. Acad. Sci. U.S.A. 91:11393–11397

Chung, J.-S., K. Sato, I. I. Dougherty, P. D. Cruz Jr, and K. Ariizumi. 2007. DC-HIL is a negative regulator of T lymphocyte activation. Blood109:4320–4327.

Doetsch, F., J. M. García-Verdugo, and A. Alvarez-Buylla. 1997. Cellular composition and three-dimensional organization of the subventricular germinal zone in the adult mammalian brain. J. Neurosci. 17:5046–5061.

Furochi, H., S. Tamura, K. Takeshima, K. Hirasaka, R. Nakao, K. Kishi, and T. Nikawa. 2007b. Overexpression of osteoactivin protects skeletal muscle from severe degeneration caused by long-term denervation in mice. J. Med. Invest. 54:248–254.

Furochi, H., S. Tamura, M. Mameoka, C. Yamada, T. Ogawa, K. Hirasaka, Y. Okumura, T. Imagawa, S. Oguri, K. Ishidoh, et al. 2007a. Osteoactivin fragments produced by ectodomain shedding induce MMP-3 expression via ERK pathway in mouse NIH-3T3 fibroblasts. FEBS Lett. 581:5743–5750.

Goehler, L. E., A. Erisir, and R. P. A. Gaykema. 2006. Neural-immune interface in the rat area postrema. Neuroscience140:1415–1434.

Golub, E. I., H. Kim, and D. J. Volsky. 1989. Transfection of DNA into adherent cells by DEAE-dextran/DMSO method increases drastically if the cells are removed from surface and treated in suspension. Nucleic Acids Res. 17:4902.

Haralanova-Ilieva, B., G. Ramadori, and T. Armbrust. 2005. Expression of osteoactivin in rat and human liver and isolated rat liver cells. J. Hepatol. 42:565–572.

Hoashi, T., S. Sato, Y. Yamaguchi, T. Passeron, K. Tamaki, and V. J. Hearing. 2010. Glycoprotein nonmetastatic melanoma protein b, a melanocytic cell marker, is a melanosome-specific and proteolytically released protein. FASEB J. 24:1616–1629.

International Parkinson's Disease Genomics Consortium (IPDGC), and Wellcome Trust Case Control Consortium 2 (WTTCCC2). 2011. A two-stage meta-analysis identifies several new loci for Parkinson's disease. PLoS Genet. 7:e1002142.

Kettenman, H., U.-K. Hanisch, M. Noda, and A. Verkhratsky. 2011. Physiology of microglia. Physiol. Rev. 91:461–553.

Kriegstein, A. R., and M. Götz. 2003. Radial glia diversity: a matter of cell fate. Glia43:37–43.

Kuan, C.-T., K. Wakiya, J. M. Dowell, J. E. Herndon II, D. A. Reardon, M. W. Graner, G. J. Riggins, C. J. Wikstrand, and D. D. Bigner. 2006. Glycoprotein nonmetastatic melanoma protein B, a potential molecular therapeutic target in patients with glioblastoma multiforme. Clin. Cancer Res. 12:1970–1982.

Kuan, C.-T., K. Wakiya, S. T. Keir, J. Li, J. E. Herndon II, I. Pastan, and D. D. Binger. 2011. Affinity-matured anti-glycoprotein NMB recombinant immunotoxins targeting malignant gliomas and melanomas. Int. J. Cancer129:111–121.

Li, B., A. P. Castano, T. E. Hudson, B. T. Nowlin, S.-L. Lin, J. V. Bonventure, K. D. Swanson, and J. S. Duffield. 2010. The melanoma-associated transmembrane glycoprotein Gpnmb controls trafficking of cellular debris for degradation and is essential for tissue repair. FASEB J. 24:4767–4781.

Liu, X., A. J. Bolteus, D. M. Balkin, O. Henschel, and A. Bordey. 2006. GFAP-expressing cells in the postnatal subventricular zone display a unique glial phenotype intermediate between radial glia and astrocytes. Glia54:394–410.

Loging, W. T., A. Lal, I.-M. Siu, T. L. Loney, C. J. Wikstrand, M. A. Marra, C. Prange, D. D. Bingner, R. L. Strausberg, and G. J. Riggins. 2000. Identifying potential tumor markers and antigens by database mining and rapid expression screening. Genome Res. 10:1393–1402.

Mizushima, S., and S. Nagata. 1990. pEF-BOS, a powerful mammalian expression vector. Nucleic Acids Res. 18: 5322.

Nakamura, A., A. Ishii, C. Ohata, and T. Komurasaki. 2007. Early induction of osteoactivin expression in rat renal tubular epithelial cells after unilateral ureteral obstruction. Exp. Toxicol. Pathol. 59:53–59.

Naumovski, L., and J. R. Junutula. 2010. Glembatumumab vedotin, a conjugate of an anti-glycoprotein non-metastatic melanoma protein B mAb and monomemthyl auristatin E for the treatment of melanoma and breast cancer. Curr. Opin. Mol. Ther. 12:248 –257.

Ogawa, T., T. Nikawa, H. Furochi, M. Kosyoji, K. Hirasaka, N. Suzue, K. Sairyo, S. Nakano, T. Yamaoka, M. Itakura, et al. 2005. Osteoactivin upregulates expression of MMP-3 and MMP-9 in fibroblasts infiltrated into denervated skeletal muscle in mice. Am. J. Cell Physiol. 289:697–707.

Onaga, M., A. Ido, S. Hasuike, H. Uto, A. Moriuchi, K. Nagata, T. Hori, K. Hayash, and H. Tsubouchi. 2003. Osteoactivin expressed during cirrhosis development in rats fed a choline-deficient, L-amino acid-defined diet, accelerates motility of hepatoma cells. J. Hepatol. 39:779–785.

Osamura, N., K. Ikeda, T. Ito, H. Higashida, K. Tomita, and S. Yokoyama. 2005. Induction of interleukin-6 in dorsal root ganglion neurons after gradual elongation of rat sciatic nerve. Exp. Neurol. 195:61–70.

Owen, T., S. L. Smock, S. Prakash, L. Pinder, D. Brees, D. Krull, T. A. Castleberry, Y. C. Clancy, S. C. Marks Jr, F. F. Safadi, et al. 2003. Identification and characterization of the genes encoding human and mouse osteoactivin. Crit. Rev. Eukaryot. Gene Expr. 13:205–220.

Pahl, M. V., N. D. Vaziri, J. Yuan, and S. G. Adler. 2010. Upregulation of monocyte/macrophage HGFIN (Gpnmb/osteoactivin) expression in end-stage renal disease. Clin. J. Am. Soc. Nephrol. 5:56–61.

Patel-Chamberlin, M., Y. Wang, B. Satirapoj, L. M. Phillips, C. C. Nast, T. Dai, R. A. Watkins, X. Wu, R. Natarajan, A. Leng, et al. 2011. Hematopoietic growth factor inducible neurokinin-1 (Gpnmb/Osteoactivin) is a biomarker of progressive renal injury across species. Kidney Int. 79:1138–1148.

Pollack, V. A., E. Alvarez, K.F. Tse, M. Y. Torgov, S. Xie, S. G. Shenoy, J. R. MacDougall, S. Arrol, H. Zhong, R. W. Gerwien, et al. 2007. Treatment parameters modulating regression of human melanoma xenografts by an antibody-drug conjugate (CR011-vcMMAE) targeting GPNMB. Cancer Chemother. Pharmacol. 60:423–435.

Qian, X., E. Mills, M. Torgov, W. J. LaRochelle, and M. Jeffers. 2008. Pharmacologically enhanced expression of GPNMB increases the sensitivity of melanoma cells to the CR011-vcMMAE antibody-drug conjugate. Mol. Oncol. 2:81–93.

Rakic, P. 2003. Elusive radial glial cells: historical and evolutionary perspective. Glia43:19–32.

Rich, J. N., Q. Shi, M. Hjelmeland, T. J. Cummings, C.-T. Kuan, D. D. Binger, C. M. Counter, and X.-F. Wang. 2003. Bone-related genes expressed in advanced malignancies induce invasion and metastasis in a genetically defined human cancer model. J. Biol. Chem. 278:15951–15957.

Ripoll, V. M., K. M. Irvine, T. Ravasi, M. J. Sweet, and D. A. Hume. 2007. *Gpnmb* is induced in macrophages by IFN-γ and lipopolysaccharide and acts as a feedback regulator of proinflammatory responses. J. Immunol. 178:6557–6566.

Rose, A. A. N., A.-A. Grosset, Z. Dong, C. Russo, P. A. MacDonald, N. R. Bertos, Y. St-Pierre, R. Simantov, M. Hallett, M. Park, et al. 2010b. Glycoprotein nonmetastatic B is an independent prognostic indicator of recurrence and novel therapeutic target in breast cancer. Clin. Cancer Res. 16:2147–2156.

Rose, A. A. N., and P. Siegel. 2010. Emerging therapeutic targets in breast cancer bone metastasis. Future Oncol. 6:55–74.

Rose, A. A. N., M. G. Annis, Z. Dong, F. Pepin, M. Hallett, M. Park, and P. M. Siegel. 2010a. ADAM10 releases a soluble form of the GPNMB/osteoactivin extracellular domain with angiogenic properties. PLoS One5:e12093.

Safadi, F. F., J. Xu, S. L. Smock, M. C. Rico, T. A. Owen, and S. N. Popoff. 2002. Cloning and characterization of osteoactivin, a novel cDNA expressed in osteoblasts. J. Cell. Biochem. 84:12–26.

Selim, A. A., J. L. Castaneda, T. A. Owen, S. N. Popoff, and F. F. Safadi. 2007. The role of osteoactivin-derived peptides in osteoclast differentiation. Med. Sci. Monit. 13:BR259–BR270.

Selim, A. A., S. M. Abdelmagid, R. A. Kanaan, S. L. Smock, T. A. Owen, S. N. Popoff, and F. F. Safadi. 2003. Anti-osteoactivin inhibits osteoblast differentiation and function *in vitro*. Crit. Rev. Eukaryot. Gene Expr. 13:265–275.

Selim, A. A. 2009. Osteoactivin bioinformatic analysis: prediction of novel functions, structural features, and modes of action. Med. Sci. Monit. 15:MT19–MT33.

Sheng, M. H.-C., J. E. Wergedal, S. Mohan, and K.-H. W. Lau. 2008. Osteoactivin is a novel osteoclastic protein and plays a key role in osteoclast differentiation and activity. FEBS Lett. 582:1451–1458.

Shikano, S., B. Bonkobara, P. K. Zukas, and K. Ariizumi. 2001. Molecular cloning of a dendritic cell-associated transmembrane protein, DC-HIL, that promotes RGD-dependent adhesion of endothelial cells through recognition of heparan sulfate proteoglycans. J. Biol. Chem. 276:8125–8134.

Spassky, N., F.T. Merkle, N. Flames, A. D. Tramontin, J. M. García-Verdugo, and A. Alvarez-Buylla. 2005. Adult ependymal cells are postmitotic and are derived from radial glial cells during embryogenesis. J. Neurosci. 25:10–18.

Tomihari, M., J.-S. Chung, H. Akiyoshi, P. D. Cruz Jr, and K. Ariizumi. 2010. DC-HIL/Glycoprotein nmb promotes growth of melanoma in mice by inhibiting the activation of tumor-reactive T cells. Cancer Res. 70:5778–5787.

Tse, K. F., M. Jeffers, V. A. Pollack, D. A. McCabe, M. L. Shadish, N. V. Khramtsov, C. S. Hackett, S. G. Shenoy, B. Kuang, F. L. Boldog, et al. 2006. CR011, a fully human monoclonal antibody-auristatin E conjugate, for the treatment of melanoma. Clin. Cancer Res. 12:1373–1382.

Tyburczy, M. E., K. Kotulska, P. Pokarowski, J. Mieczkowski, W. Grajkowska, M. Roszkowski, S. Jozwiak, and B. Kaminska. 2010. Novel proteins regulated by mTOR in subependymal giant cell astrocytomas of patients with tuberous sclerosis complex and new therapeutic implications. Am. J. Pathol. 176:1878–1890.

Vallières, L., and S. Rivest. 1997. Regularion of the genes encoding interleukin-6, its receptor, and gp130 in the rat brain in response to the immune activator lipopolysaccharide and the proinflammatory cytokine intrleukin-1β. J. Neurochem. 69:1668–1683.

Wang, D. D., and A. Bordey. 2008. The astrocyte odyssey. Prog. Neurobiol. 86:342–367.

Weterman, M. A. J., N. Ajubi, I. M. R. van Dinter, W. G. J. Degen, G. N. P. van Muijen, D. J. Rutter, and H. P. J. Bloemers. 1995. *nmb*, a novel gene, is expressed in low-metastatic human melanoma cell lines and xenografts. Int. J. Cancer60:73–81.

Williams, M. D., B. Esmaeli, A. Soheili, R. Simantov, D. S. Gombos, A. Y. Bedikian, and P. Hwu. 2010. GPNMB expression in uveal melanoma: a potential for targeted therapy. Melanoma. Res. 20:184–190.

Supporting Information

Additional Supporting Information may be found in the on-line version of this article:

Figure. S1. Characterization of Gpnmb-IR cells in cortical layer VI with multiple markers.
Figure. S2. Distribution of Gpnmb-IR in the olfactory bulb.
Figure. S3. Distribution of Gpnmb-IR in the striatum.
Table S1. Distribution of Gpnmb-immunoreactivity in the Adult Rat Brain.

Please note: Wiley-Blackwell is not responsible for the content or functionality of any supporting materials supplied by the authors. Any queries (other than missing material) should be directed to the corresponding author for the article.